cules. By increasing the pressure, the number of dissociated molecules (and thus of the protonic carriers) increase exponentially across the molecular-ionic cross-over. In the ionic regime all the protons contribute equally to the conductivity, and a further increase in pressure increases the proton mobility without changing the number of carriers.

Moving deeper into the planet, the ice core boundary is met at 600 GPa and 7000 K according to the presently accepted planetary isentrope (*2*). At these conditions we predict water and ammonia to be metallic (*24*). This may have at least two consequences. First, the dynamo generation of the magnetic field should include the contribution of the high electronic conductivity due to the metallic liquid in the inner part of the ice layer, and the lower electrical conductivity due to the proton mobility in the electronically insulating liquid in the outer part of the ice layer. Second, a metallic state of water may affect its solubility with hydrogen and rocks. This may alter current views on the partitioning of these materials in the deepest regions of the ice layer. However, alternative models of the giant planets have been proposed which assume that above 150 GPa the interior is isothermal at a temperature of ≈5000 K (*2*, *25*). In this case the ices will remain electronically insulating in the whole planet.

References and Notes

1. W. B. Hubbard, *Science* **214**, 145 (1981).
2. _____, M. Podolak, D. J. Stevenson, in *Neptune and Triton*, D. P. Cruikshank, Ed. (Univ. of Arizona Press, Tucson, AZ, 1995), pp. 109–138.
3. N. F. Ness *et al.*, *Science* **233**, 85 (1986); *ibid.* **246**, 1473 (1989).
4. R. L. Kirk and D. J. Stevenson, *Astrophys. J.* **316**, 836 (1987).
5. W. J. Nellis *et al.*, *Science* **240**, 779 (1988).
6. D. J. Stevenson, *Rep. Prog. Phys.* **46**, 555 (1983).
7. W. J. Nellis, N. C. Holmes, A. C. Mitchell, D. C. Hamilton, M. Nicol, *J. Chem. Phys.* **107**, 9096 (1997).
8. W. B. Hubbard *et al.*, *Science* **253**, 648 (1991).
9. F. Ancilotto, G. L. Chiarotti, S. Scandolo, E. Tosatti, *ibid.* **275**, 1288 (1997).
10. M. Benoit, D. Marx, M. Parrinello, *Nature* **392**, 258 (1998); M. Bernasconi, P. L. Silvestrelli, M. Parrinello, *Phys. Rev. Lett.* **81**, 1253 (1998).
11. M. Benoit, M. Bernasconi, P. Focher, M. Parrinello, *Phys. Rev. Lett.* **76**, 2934 (1996).
12. P. Demontis, R. L. LeSar, M. L. Klein, *ibid.* **60**, 2284 (1988).
13. R. Car and M. Parrinello, *ibid.* **55**, 2471 (1985).
14. Previous simulations (*9*) have shown that at these conditions methane, the third component of the ice layer, transforms into saturated hydrocarbons of heavier molecular weight that do not contribute to the electrical conductivity.
15. P. Focher, G. L. Chiarotti, M. Bernasconi, E. Tosatti, M. Parrinello, *Europhys. Lett.* **36**, 345 (1994); M. Bernasconi *et al.*, *J. Phys. Chem. Solids* **56**, 510 (1995).
16. We used a gradient correction to the local-density approximation (*26*) that accurately describes the hydrogen bonding (*27*). Norm-conserving pseudopotentials (*28*) and an integration time step of 0.075 fs were used. The electronic wavefunctions were expanded in plane waves up to a kinetic energy cutoff of 70 Ry and assumed to have the same periodicity of the simulation cell.
17. P. V. Hobbs, *Ice Physics* (Clarendon, Oxford, 1974).
18. K. R. Hirsch and W. B. Holzapfel, *Phys. Lett.* **101**, 142 (1984); Ph. Pruzan *et al.*, *J. Chem. Phys.* **99**, 9842 (1993); K. Aoki *et al.*, *Phys. Rev. Lett.* **76**, 784 (1996); A. F. Goncharov *et al.*, *Science* **273**, 218 (1996). The existence of ice X, first inferred from spectroscopy but not yet observed directly, has been confirmed by ab initio molecular dynamics (*10*), which yield a transition pressure of 102 GPa (72 GPa) by treating the proton as a classical (quantum) particle.
19. J. S. Loveday *et al.*, *Phys. Rev. Lett.* **76**, 74 (1996).
20. W. B. Hubbard and J. J. MacFarlane, *J. Geophys. Res.* **85**, 225 (1980).
21. Uncertainties on phase boundaries are related to the limited simulation times and cell sizes. They are estimated from the simulated hysteresis loop.
22. The isentropes of Uranus and Neptune are believed to be similar (*8*, *29*).
23. The ionic conductivity has been computed from the proton diffusion coefficient, the effective charge, and the Nerst-Einstein relation. The proton effective charge is $\sim+e$ as obtained from the calculation of the change in polarization associated to diffusion by the Berry-phase formalism of (*30*).
24. Although we have not performed simulations above 300 GPa, where we found a metallization temperature for water of 7000 K, the metallization temperature is expected to decrease with pressure (as it does in going from 150 to 300 GPa).
25. W. B. Hubbard, *Science* **275**, 1279 (1997).
26. A. D. Becke, *Phys. Rev.* **A 38**, 3098 (1988); C. Lee, W. Yang, R. G. Parr, *ibid.* **B 37**, 785 (1988).
27. M. Sprik, J. Hütter, M. Parrinello, *J. Chem. Phys.* **105**, 1142 (1996).
28. N. Troullier and J. L. Martins, *Phys. Rev.* **B 43**, 1993 (1991).
29. M. Podolak, A. Weizman, M. Morley, *Planet. Space Sci.* **43**, 1517 (1995).
30. R. D. King-Smith and D. Vanderbilt, *Phys. Rev.* **B 47**, 1651 (1993).
31. R. J. Hemley *et al.*, *Nature* **330**, 737 (1987).
32. F. Datchi, P. Loubeyre, R. LeToullec, *Rev. High Pressure Sci. Technol.* **7**, 778 (1998).
33. A. C. Mitchell and W. J. Nellis, *J. Chem. Phys.* **76**, 6273 (1982).
34. Calculations for water at 300 K and 66 GPa give ρ = 2.86 g/cm^3, in agreement with x-ray data (2.83 g/cm^3) (*31*).

35. We acknowledge partial support from Istituto Nazionale per La Fisica della Materia and Ministero dell' Universitá e della Ricerca Scientifica e Technologica.

12 August 1998; accepted 17 November 1998

Liquid Morphologies on Structured Surfaces: From Microchannels to Microchips

Hartmut Gau, Stephan Herminghaus, Peter Lenz, Reinhard Lipowsky*

Liquid microchannels on structured surfaces are built up using a wettability pattern consisting of hydrophilic stripes on a hydrophobic substrate. These channels undergo a shape instability at a certain amount of adsorbed volume, from a homogeneous state with a spatially constant cross section to a state with a single bulge. This instability is quite different from the classical Rayleigh Plateau instability and represents a bifurcation between two different morphologies of constant mean curvature. The bulge state can be used to construct channel networks that could be used as fluid microchips or microreactors.

Structured surfaces that exhibit lateral patterns of varying wettability can be produced by different techniques, such as microcontact printing (*1, 2*), vapor deposition (*3*), and photolithography (*4, 5*). It appears very promising to use such patterns as templates for three-dimensional (3D) structures that extend into adjacent soft matter phases.

In the present study, we created a pattern with a high wettability contrast for water. In order to obtain stripes that are as hydrophilic as possible, we generated the wettable regions by thermal vapor deposition of MgF_2 onto a hydrophobic silicone rubber or a thiolated gold substrate through appropriate masks. Both substrates exhibited the same hydrophobicity, as measured by the corresponding contact angles. The masks consisted of grids that are commercially available for electron microscopy and yielded arrays of parallel stripes with a width of a few tens of micrometers, separated by hydrophobic stripes of the same width. The thickness of the MgF_2 layer was typically 20 nm. The pattern was exposed to water vapor at a humidity of 40%. When cooled to the temperature 5°C below the dew point, the water condenses on the wettable hydrophilic regions, producing liquid microchannels.

If one deposits a small amount of water on the hydrophilic MgF_2 stripes, the microchannels are homogeneous and are shaped as cylinder segments with a constant cross section (Fig. 1A). As more and more water is adsorbed onto these channels, their volume grows until they undergo a sudden transition to a morphologically different state, and each channel then exhibits a single bulge with a characteristic shape (Fig. 1B).

Experimentally, we used optical microscopy in order to observe the contours of the

H. Gau and S. Herminghaus, Max-Planck-Institute (MPI) of Colloids and Interfaces, Rudower Chaussee 5, D-12489, Berlin-Adlershof, Germany. P. Lenz and R. Lipowsky, MPI of Colloids and Interfaces, Kantstrasse 55, D-14513 Teltow-Seehof, Germany.

*To whom correspondence should be addressed.

microchannel shape when projected perpendicular to the substrate surface (Fig. 1 and Fig. 2D) and evanescent wave microscopy to measure the position of the contact lines of the channel along the substrate (Fig. 2E). In the latter technique, the incoming light beam is totally reflected at the substrate and creates an evanescent wave very close (<100 nm) to it. For the thiolated gold substrate, this evanescent wave excites surface plasmons within the dry surface domains, and the latter domains appear dark in the microscopic image.

Theoretically, we calculated the full 3D shape of the channel (Fig. 2A), from which we determined its projected shape (Fig. 2B) and the position of the contact line (Fig. 2C). Direct inspection of Fig. 2 shows that the experimental and the theoretical shapes are in good agreement.

The surface channel instability in Figs. 1 and 2 is rather different from the classical Rayleigh Plateau instability (*6*), which is characterized by the decay of a free-standing cylinder into a periodic array of many droplets. This instability has been studied for liquid jets (*7*), for liquid films coating thin fibers (*8*), and for long cylindrical vesicles (*9*). In contrast, the instability discussed here leads to a single bulge for each cylindrical channel. Furthermore, whereas the free-standing cylinder will always undergo a Rayleigh Plateau instability, the homogeneous channel turns out to be stable as long as its volume is sufficiently small.

Theoretically, the shapes of the channels are given by constant mean curvature surfaces, which are constrained by the domain boundaries within the structured substrate. If the contact lines are forced to sit on top of these domain boundaries (that is, for a hard constraint), differential geometry provides a few general theorems that ensure the existence of such surfaces as long as the mean curvature is sufficiently small (*10, 11*). Our theoretical work embodies two general features not covered by these theorems: (i) The control parameter is the overall volume of the channel rather than the mean curvature of its surface; and (ii) for the system parameters studied here, the bulge state is characterized by a contact line that detaches itself from the boundary of the hydrophilic surface domain and makes an excursion across the hydrophobic surface (Fig. 2, C and E).

Our theory depends only on two material parameters; that is, on two contact angles. All other parameters are related to the geometry of the pattern: the width and length of the striped surface domains and the total volume of liquid that is deposited on the stripe. All of these parameters are directly accessible to experiments. Thus, the theoretical shapes shown in Fig. 2 do not contain any fit parameter.

In order to understand the character of this instability, one must examine the contact angle between the liquid-vapor interface and the substrate surface. For a homogeneous solid substrate, the contact angle θ satisfies the Young equation $\cos(\theta) = (\sigma_{VS} - \sigma_{LS})/\sigma_{LV}$, where σ_{VS}, σ_{LS}, and σ_{LV} are the vapor-solid, liquid-solid, and liquid-vapor interfacial tensions, respectively (*12*). Thus, for the hydrophobic silicone rubber or the thiolated gold substrate ($S = \delta$) as considered here, one would have the relatively large contact angle $\theta = \theta_\delta \simeq 108°$. However, in the presence of the hydrophilic surface stripes ($S = \gamma$), the water starts to condense onto these stripes, and the resulting droplets have the relatively small contact angle $\theta = \theta_\gamma \lesssim 5°$, as we could infer from interference fringes observed under the optical microscope.

As more water condenses onto the stripes, these droplets coalesce until the hydrophilic stripes are completely covered by water, and the contact lines of these channels are located at the surface domain boundaries; that is, at the boundaries of the stripes. As we continue to add water onto the surface, the channels grow thicker, but they still have the shape of cylindrical caps and their contact lines are still pinned at the domain boundaries. This implies that the contact angle θ of the water channels no longer satisfies the Young equation but the inequality $\theta_\gamma < \theta < \theta_\delta$ (*13*). Therefore, as the water channels grow thicker, their contact angle increases in a continuous fashion.

Consider a homogeneous channel with constant cross section and constant contact angle θ. In order to determine its stability, one must study shape deformations that conserve the liquid volume and leave the position of the contact line unchanged. From this linear stability analysis, one finds that the cylinder is locally stable for contact angle $\theta < 90°$ but unstable for $\theta > 90°$, provided that the wavelength λ of the shape deformation exceeds a certain threshold value λ_c given by

$$\lambda_c = \left[\frac{\pi/2}{\theta^2 - (\pi/2)^2}\right]^{1/2} \frac{\theta}{\sin(\theta)}\, a_\gamma \qquad (1)$$

which depends on θ and on the width a_γ of the hydrophilic stripe.

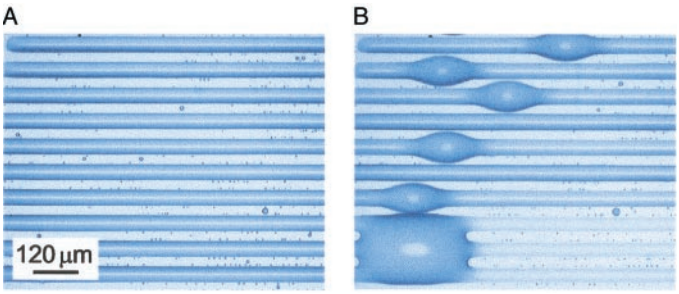

Fig. 1. Microchannels of water as observed by optical microscopy. (**A**) Low-coverage regime. The channels have a constant cross section and a small contact angle. (**B**) High-coverage regime. The channels developed a single bulge as soon as the contact angle exceeded a certain characteristic value. If two bulges of two neighboring channels are in close proximity, they may merge with each other (see the larger structure in the lower left corner).

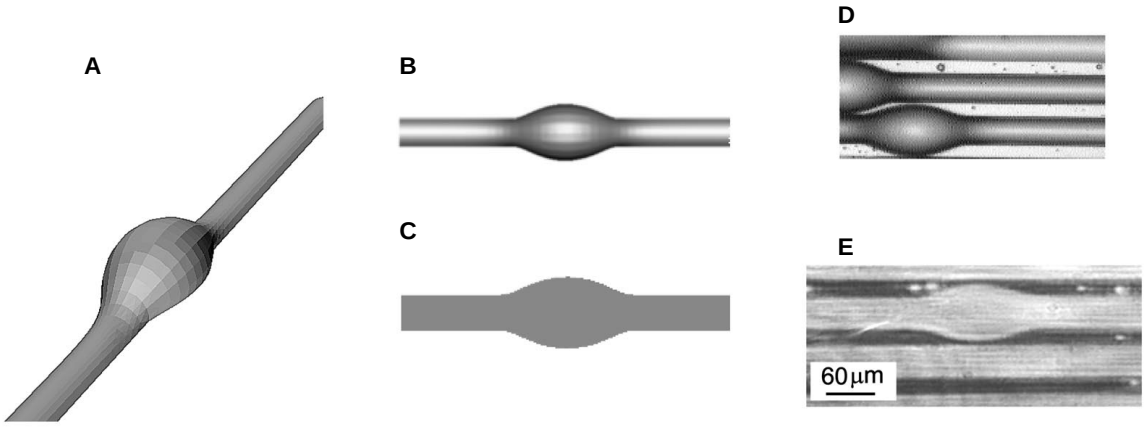

Fig. 2. (**A**) Bulge state of a microchannel as determined theoretically. (**B** and **D**) Projection of the shape perpendicular to the substrate. (**C** and **E**) Location of the contact line, which makes an excursion into the hydrophobic surface domains. (B) and (C) were obtained from the theoretical shape; (D) and (E) were obtained from the experimental observations.

We conclude that the cylindrical channel is unstable if the contact angle exceeds 90°. Further insight into the new state that arises out of this instability can be obtained from a somewhat crude approximation in which one replaces the hydrophilic stripe by a linear array of N circular domains that all have the same diameter. We place the same amount of liquid onto these domains and let the resulting droplets exchange liquid among each other. In this way, the liquid channel is approximated by a linear chain of N droplets that have the form of spherical caps.

All droplets must have the same mean curvature M as given by the Laplace equation $P_L - P_V = 2M\sigma_{LV}$, where P_L, P_V, and σ_{LV} denote the liquid and vapor pressure and the tension of the liquid-vapor interface, respectively. For a spherical cap, M is simply the inverse of the radius of the sphere. In addition, the contact area of these droplets is essentially fixed to be identical with the area of the circular surface domains. This implies that the droplet chain can only consist of two different types of droplets: small ones with contact angle θ_{sm} and large ones with contact angle θ_{la}. If one combines one small droplet with one large droplet in such a way that they are pasted together along their flat contact areas, one obtains a complete sphere, which implies $\theta_{sm} + \theta_{la} = 180°$.

One must now consider different arrangements consisting of N_{sm} small and N_{la} large droplets with $N_{sm} + N_{la} = N$ (Fig. 3). A systematic calculation of the corresponding free energies (*13*) shows that only two of these possible arrangements represent stable or metastable states—(i) the homogeneous droplet pattern consisting of a chain of identical droplets (Fig. 3A) and (ii) heterogeneous droplet patterns, consisting of only one large droplet and $N - 1$ small ones (Fig. 3B). In terms of the original channel geometry, these two states correspond to the homogeneous channel state and the heterogeneous channel state with only one bulge.

Calculation of the free energies of the different droplet patterns leads to the bifurcation diagram in Fig. 4A. The bifurcation is discontinuous and exhibits a hysteresis loop. Thus, the homogeneous droplet pattern is metastable up to a certain maximal volume, and the heterogeneous pattern with one large droplet is metastable down to a certain minimal volume. For the systems considered here, this minimal volume is very close to the bifurcation point and the hysteresis loop is rather asymmetrical. The maximal volume of the homogeneous pattern, on the other hand, corresponds to droplets with a contact angle of 90°, which is precisely the same value as that obtained from the linear stability analysis of the homogeneous channel. Therefore, within the approximation just discussed, the channel undergoes a discontinuous bifurication from a homogeneous state to a heterogeneous state with one bulge.

To calculate the precise shape of the bulge state and the precise bifurcation diagram, we determined numerically the minima of the channel free energy and the corresponding constant mean curvature surfaces. We used available software packages such as Surface Evolver (*14*) and developed a special code adapted to the channel geometry. The initial configuration of the liquid surface was chosen to be a homogeneous cylindrical cap that was discretized and covered by a net of triangles. This surface shape was then perturbed by displacements along the radial direction of the cylinder. A gradient method was used to determine the local minima of the channel free energy. In this way, we obtained the shapes in Fig. 2 and the bifurcation diagram in Fig. 4B.

The bifurcation structure underlying the instability described here implies that this instability is rather general. Our calculations show that it applies to any liquid on any striped surface, provided that the contact angle of the lyophilic stripes is sufficiently small and the stripe is sufficiently long. The presence of this instability makes it impossible to construct long homogeneous channels with a contact angle that exceeds 90°. However, the bulge arising from this instability may coalesce with a neighboring channel and thus lead to a microbridge between two channels (Fig. 1B).

In Fig. 1B, these bridges are stable, because the stripes between the channels are sufficiently

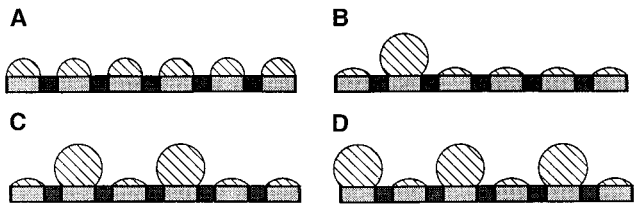

Fig. 3. Possible droplet patterns on a linear chain of circular domains. Because of the Laplace equation, all droplets must have the same mean curvature, which implies that the small and the large droplet must form a complete sphere when pasted together along their flat contact areas. All droplet patterns, such as (**C**) and (**D**), that contain more than one large droplet are unstable and must decay into the homogeneous pattern (**A**) or into the heterogeneous pattern (**B**) with only one large droplet.

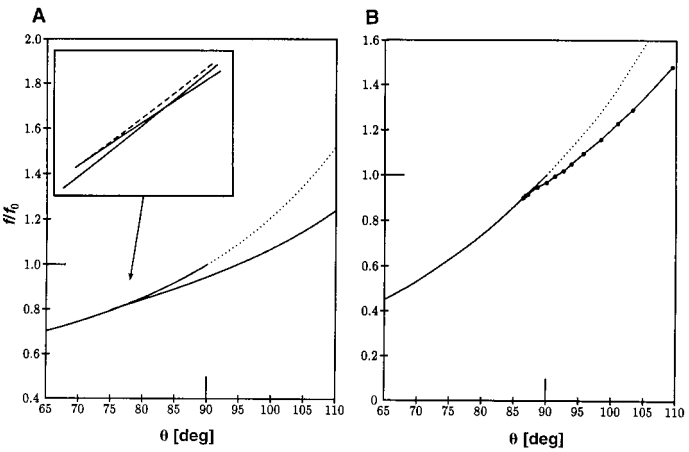

Fig. 4. Bifurcation of channel states: free energy f/f_o as a function of the angle θ. For the homogeneous channel, θ is the actual contact angle; for the bulge state, θ is the contact angle of the homogeneous channel, which has the same volume as the bulge state. The scale f_o is the free energy of the homogeneous channel with $\theta = 90°$. At $\theta = \theta_* < 90°$, the homogeneous state becomes metastable, and the state with a single bulge becomes the state of lowest free energy. At $\theta = \theta_{max} = 90°$, the homogeneous channel becomes unstable. The dotted line in (**A**) and (**B**) represents this unstable state. The dashed line in the inset of (A) corresponds to another unstable state. (A) and (B) were obtained from the approximation in Fig. 3 and from numerical minimization, respectively.

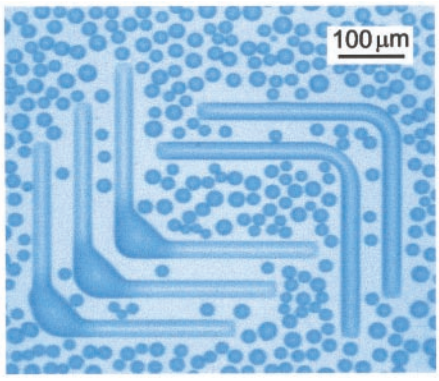

Fig. 5. Microchannels formed on striped surface domains with corners. When such a channel undergoes the shape instability described here, the bulge prefers to sit at such a corner because it can then maximize its contact with the hydrophilic stripe. If the corners are close enough to each other, two bulges in two adjacent corners will coalesce and thus form a microbridge between the two neighboring microchannels.

hydrophobic and have a relatively large width. If one reduces the hydrophobicity or the width of such a stripe, the bridge formation will nucleate a spreading process that leads to the complete coverage of the hydrophobic stripe and to the coalescence of the channels.

Wettability patterns where pairs (or multiplets) of hydrophilic stripes have a smaller hydrophobic separation could be used as fluid microchips or microreactors. First, the different channels on the stripe pairs (or multiplets) would be filled with different reactants. Secondly, the coalescence of these channels could be induced by simply increasing their volume. In this way, small amounts of reactants could be prepared in a well-mixed state without any stirring.

Stable bridges may be placed at controlled positions by using striped surface domains with a nonuniform width or with corners (Fig. 5). In this way, one may create 2D networks of microchannels. When filled with electrolytes, one obtains another type of microchip, because the channels now act as ionic conductors.

Finally, after a certain pattern of liquid channels and bridges has been created, one may want to stabilize it by freezing, polymerization, or sol-gel reactions. When the volume change at such a phase transformation is small, the shape of the liquid pattern will be conserved. In this way, one should be able to produce both rigid and soft structures with a large variety of morphologies between two and three dimensions (*15*).

References and Notes

1. G. P. Lopez, H. A. Biebuyck, C. D. Frisbie, G. M. Whitesides, *Science* **260**, 647 (1993); J. Drelich, J. D. Miller, A. Kumar, G. M. Whitesides, *Colloids Surf. A* **93**, 1 (1994).
2. F. Morhard *et al*., *Electrochem. Soc. Proc.* **97**, 1058 (1997).
3. K. Jacobs *et al*., in *Proceedings of the 2nd European Coating Symposium, Strasbourg, 1997*, in press.
4. R. Wang *et al*., *Nature* **388**, 431 (1997).
5. G. Möller, M. Harke, H. Motschmann, *Langmuir* **14**, 4955 (1998).
6. S. Chandrasekhar, *Hydrodynamic and Hydromagnetic Stability* (Dover, New York, 1981).
7. M. van Dyke, *An Album of Fluid Motion* (Parabolic Press, Stanford, CA, 1982).
8. D. Quere, J.-M. di Meglio, F. Brochard-Wyart, *Science* **249**, 1256 (1990).
9. R. Bar-Ziv and E. Moses, *Phys. Rev. Lett.* **73**, 1392 (1994); R. Goldstein, P. Nelson, T. Powers, U. Seifert, *J. Phys. II Fr.* **6**, 767 (1996).
10. M. Struwe, *Plateau's Problem and the Calculus of Variations* (Princeton Univ. Press, Princeton, NJ, 1988).
11. J. Sullivan and F. Morgan, *Int. J. Math.* **7**, 833 (1996).
12. J. S. Rowlinson and B. Widom, *Molecular Theory of Capillarity* (Clarendon, Oxford, 1982).
13. P. Lenz and R. Lipowsky, *Phys. Rev. Lett.* **80**, 1920 (1998).
14. K. Brakke, *Exp. Math.* **1**, 141 (1990).
15. Some applications of the microchannel structures discussed here have already been patented (German Patent No. 197 48 295.3).

16. We acknowledge support by the Deutsche Forschungsgemeinschaft through the Schwerpunktprogramm 1052.

14 September 1998; accepted 20 November 1998

Sum Rules and Interlayer Conductivity of High-T_c Cuprates

D. N. Basov, S. I. Woods, A. S. Katz, E. J. Singley, R. C. Dynes, M. Xu,* D. G. Hinks, C. C. Homes, M. Strongin

Analysis of the interlayer infrared conductivity of cuprate high–transition temperature superconductors reveals an anomalously large energy scale extending up to midinfrared frequencies that can be attributed to formation of the superconducting condensate. This unusual effect is observed in a variety of materials, including $Tl_2Ba_2CuO_{6+x}$, $La_{2-x}Sr_xCuO_4$, and $YBa_2Cu_3O_{6.6}$, which show an incoherent interlayer response in the normal state. Midinfrared range condensation was examined in the context of sum rules that can be formulated for the complex conductivity. One possible interpretation of these experiments is in terms of a kinetic energy change associated with the superconducting transition.

Interlayer electron transport in cuprate superconductors has been the focus of both experimental and theoretical efforts (*1–11*). The radical differences between the in-plane and interlayer behaviors of cuprates are most clearly illustrated in the raw reflectance $R(\omega)$ measured with polarized light of frequency ω. In high transition temperature (T_c) superconductors, the reflectance of the electric field component parallel to the CuO_2 planes shows a metallic response, whereas reflectance obtained in the polarization along the interplane c axis direction [$R_c(\omega)$] is like that of ionic insulators with characteristic phonon peaks in the far infrared (IR), as shown in Fig. 1 for $Tl_2Ba_2CuO_{6+x}$ (Tl2201). Below T_c a sharp plasma edge at $\omega = 37$ cm^{-1} (in Tl2201) emerges out of a nearly "insulating" normal state spectrum because superconducting (SC) currents flow along all crystallographic directions. In other cuprate compounds, this feature appears at 10 to 200 cm^{-1} (*2–4, 12–15*). A collective (Josephson-like) mode associated with pair tunneling between CuO_2 layers implies a plasma edge in the IR reflectance with the frequency position of the minimum in $R_c(\omega)$ being proportional to the square root of the superfluid density ρ_s. The magnitude of ρ_s quantifies the electronic spectral weight of the SC δ function: $\rho_s = 4\pi n_s e^2/m^*$ (*16*), where n_s is the density of SC carriers, m^* is their mass, and e is the electron charge. Although development of the plasma edge is expected based on elementary electrodynamics (*6*), formation of the SC condensate from the incoherent normal state response is an intriguing issue.

We explored the changes in incoherent c-axis conductivity below T_c in connection with the c-axis superfluid density. Our analysis uses model-independent arguments based on the oscillator strength sum rule or causality of the electromagnetic response. We found that in several high-T_c cuprates, ρ_s significantly exceeds the spectral weight missing from the real part of the conductivity in a frequency region comparable to the SC gap 2Δ. This discrepancy in spectral weight indicates that a significant fraction of ρ_s is accumulated from mid-IR frequencies. These results support the hypothesis of a kinetic energy change associated with the superconducting transition (*5, 9, 17, 18*).

We measured the c-axis response of Tl2201 at the University of California at San Diego and compared our new data with earlier results reported by Timusk's group at McMaster University for lightly underdoped $La_{2-x}Sr_xCuO_4$ (La2l4) with $T_c = 32$ K (*12*) and underdoped $YBa_2Cu_3O_{6.6}$ (Y123) with $T_c = 59$ K (*13*). $Tl_2Ba_2CuO_{6+x}$ is a structurally simple material with just one CuO_2 plane per unit cell. Single crystals were grown as described in (*7*) and exhibited a SC transition at $T_c = 81$ K with $\Delta T_c \simeq 8$ to 10 K (from magnetization). Reflectance measurements in the frequency range from 16 to 15,000 cm^{-1} were performed with an IR interferometer upgraded for spectroscopy of microsamples. Typical dimensions of the Tl2201 crystals were $0.8 \times 0.8 \times 0.075$ mm^3. A mosaic of several specimens with similar T_c and ΔT_c was used for the measurements in the energy interval down to 16 cm^{-1}. The experiment was then repeated in the range from 60 to 9000 cm^{-1} using the thickest ($\simeq$130 μm) single crystal. The difference from the mosaic spectrum did not exceed 6%. The uncertainty of the relative changes in the spectra taken at different temperatures was less than 0.5%; this latter uncertainty

D. N. Basov, S. I. Woods, A. S. Katz, E. J. Singley, R. C. Dynes, Department of Physics, University of California–San Diego, La Jolla, CA 92093–0319, USA. M. Xu, James Franck Institute, University of Chicago, Chicago, IL 60637, USA. D. G. Hinks, Department of Materials Science, Argonne National Laboratory, Argonne, IL 60439, USA. C. C. Homes and M. Strongin, Department of Physics, Brookhaven National Laboratory, Upton, NY 11973–5000, USA.

*Present address: Lucent Technologies, 2000 North Naperville Road, Naperville, IL 60566, USA.